Microfluid Nanofluid (2011) 10:1351–1357
DOI 10.1007/s10404-010-0762-5

BRIEF COMMUNICATION

Contact line dynamics of a superhydrophobic surface: application for immersion lithography

Arun Kumar Gnanappa · Evangelos Gogolides · Fabrizio Evangelista · Michel Riepen

Received: 15 August 2010 / Accepted: 14 December 2010 / Published online: 4 January 2011

Abstract The dynamic contact line behavior of water on nanotextured rough hydrophobic and superhydrophobic surfaces is studied and contrasted to smooth hydrophobic surfaces for application in immersion lithography. Liquid loss occurs at the receding meniscus when the smooth substrate is accelerated beyond a critical velocity of approximately 1 m/s. Nanotexturing the surface with average roughness values even below 10 nm results in critical velocity larger than 2.5 m/s, the upper limit of the apparatus. This unexpected increase in critical velocity is observed for both sticky hydrophobic and slippery superhydrophobic surfaces. The authors attribute this large increase in critical velocity both in increased receding contact angle and in increased slip length for such nanotextured surfaces.

Keywords Hydrophobic · Receding contact angle · Dynamic contact angle · Wetting · Water loss · Shedding

1 Introduction

Contact line of a liquid sliding on a substrate and description of the variation of receding contact angle with velocity has been studied by many groups for three quarters of a century for several applications such as industrial coating, lubrication, printer heads, film development process, etc., (Cox 1986; Voinov 1976; Podgorski et al. 2001; Eggers 2004; Snoeijer et al. 2006). In modern nanoelectronics, contact line dynamics plays a major role in improving the efficiency of immersion lithography. Immersion lithography aims to enhance resolution of optical lithography by replacing the conventional air gap between the lens and the wafer surface with a liquid that has a refractive index greater than one. Current water-based 193-nm immersion lithography can achieve feature size below 37 nm (Sanders 2010). However, the current industrial needs high throughput demands relatively large wafer scanning velocities. At higher scanning velocities, liquid loss occurs at the receding contact line of the drop confined between the substrate and the lens; this is called the critical velocity. The lost water on the wafer surface becomes the potential cause for the defects on the printed pattern (Sanders 2010; Brandl et al. 2006; Niwa et al. 2005). Researchers are working to improve the liquid loss by varying the geometry of the needle (Riepen et al. 2008), by introducing an air curtain to stabilize the meniscus (Mulkens et al. 2007), varying the height between the lens and wafer etc.

Both in theory and experiment, smooth homogeneous surfaces have been used up to now. The traditional models are based on the conditions of low Reynolds number and acceleration. Although many researchers showed that the immersion flow conditions can be directly compared with the normal water drop sliding on a slanting surface, Burnett et al. (2006) showed that the traditional sliding model can be directly implemented only for the inertia-free condition at lower velocities. Several issues of over prediction of Voinov's equation on the critical velocity have been answered by many researchers (Petrov and Petrov 1992; Podgorski et al. 2001; Burnett et al. 2005). Burnett et al. (2005 and 2006) showed that liquid loss occurs by two

A. K. Gnanappa · E. Gogolides (✉)
Institute of Microelectronics IMEL, NCSR 'Demokritos', Terma (End of) Patriarchou Gregoriou Street, Aghia Paraskevi, Attiki 15310, Greece
e-mail: evgog@imel.demokritos.gr

F. Evangelista · M. Riepen
ASML, DeRun 6500, Veldhoven, The Netherlands

conditions: film pulling and inertial instability. Film pulling occurs when the dynamic receding contact angle approaches zero and a thin layer of fluid is pulled out behind the receding meniscus. This type of failure is commonly seen in hydrophilic surfaces. Liquid loss by inertial instability occurs when the water in the meniscus cannot be contained by surface tension. This type of failure is frequently seen in hydrophobic surfaces at higher velocities (Shedd et al. 2006). The very recent model, Schuetter et al. (2007) developed a semi empirical model based on his study with liquids of various viscosity and surface tension for predicting the liquid loss in the inertial regime for the smooth homogeneous surface. According to Schuetter et al. (2007), critical velocity V_{cr} is given as;

$$V_{cr} = (V_{vi}^{-m} + V_{in}^{-m})^{-\frac{1}{m}} \quad (1)$$

$$V_{vi} = \frac{1}{9\ln(h/L_s)}\frac{\gamma}{\mu}\theta_{sr}^3 \quad (2)$$

$$V_{in} = C_2\left(\frac{\gamma}{\rho\kappa^{-1}}\right)^{3/4}\left(\frac{\gamma}{\mu}\right)^{1/4}\sin^{3/4}\left(\frac{\theta_{sr}}{2}\right) \quad (3)$$

V_{vi} is the critical velocity in the viscous regime approximated by Eq. 2 known the Voinov's equation. Here 'h' is the height between the lens and the substrate, L_s is the slip length, V_{in} is the critical velocity in the inertial regime, $m = 5$ and $C_2 = 1.05$ are empirical constants, γ is the surface tension, μ is the dynamic viscosity, θ_{sr} is the static receding angle, and κ^{-1} is the capillary length given as

$$\kappa^{-1} = \sqrt{\frac{\gamma}{\rho g}} \quad (4)$$

Equations 2 and 3 both show that the critical velocity is a strong increasing function of θ_{sr} as well as an increasing function of slip length (L_s).

While the above results have been obtained for smooth surfaces, a less studied aspect of contact line behavior is the critical velocity on rough hydrophobic and superhydrophobic surfaces, for which obviously these models have not yet been validated. Such surfaces show increased contact angle both in the Wenzel and the Cassie–Baxter regime, and in addition, show greatly enhanced slip length especially in the Cassie–Baxter regime. They are thus good candidates for increasing the critical velocity. Here the contact line dynamics of rough hydrophobic/superhydrophobic surfaces will be studied. Although the actual photoresist surface in immersion lithography cannot easily be modified to become superhydrophobic, the chuck area surrounding the wafer could benefit of a water repellent coating. The scanning process starts from outside the wafer on the actual chuck surface and accelerates toward the wafer. Superhydrophobic chuck area could largely improve

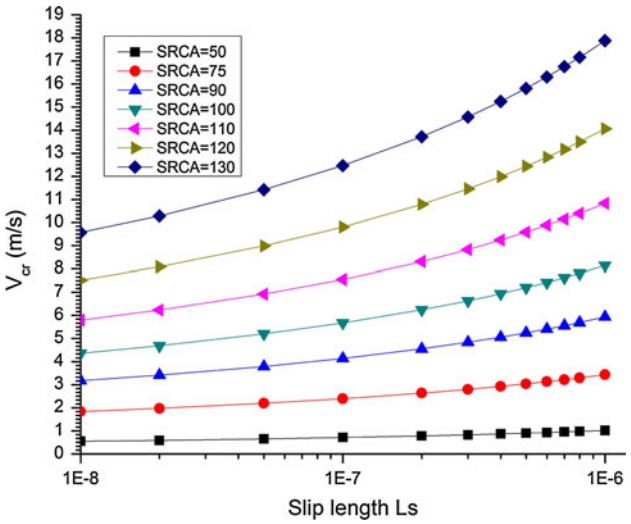

Fig. 1 Critical velocity versus slip length for various static receding contact angle

the critical velocity and hence increase in the processing speed.

Before proceeding, the authors present some examples of application of Eq.2. A small increase in static receding contact angle (SRCA) will result in increased V_{cr}. In addition, an increase of slip length L_s by a factor of 10 will result in doubling of V_{cr}. It is well known that a rough hydrophobic surface whether in the Wenzel or the Cassie state will show an increased SRCA. Thus, one way to increase V_{cr} would be to roughen the surface while keeping it hydrophobic. In addition, when a surface becomes superhydrophobic, a dramatic increase of slip length is observed (Gogte et al. 2005; Choi et al. 2006). Petrov 1992 showed that the typical range of slip length is in the range of 0.33–10 nm for predicting the critical velocity on a homogeneous smooth surface, while slip lengths in the range of few hundreds of nm have been observed on superhydrophobic surfaces with similar random roughness (Joseph et al. 2005).

Figure 1 shows the critical velocity for various slip length and static receding angle derived from Eq. 2. This plot also shows the significance of both slip length and static receding angle increases. Notice that the effect of slip length is stronger for higher contact angles, i.e., on hydrophobic and superhydrophobic surfaces. Since there is no literature on using superhydrophobic surface for immersion lithography, the authors will attempt here the first to their knowledge such study.

2 Experimental apparatus and processes

The dynamic contact line study has been performed at ASML research laboratories by means of a turn table set-up

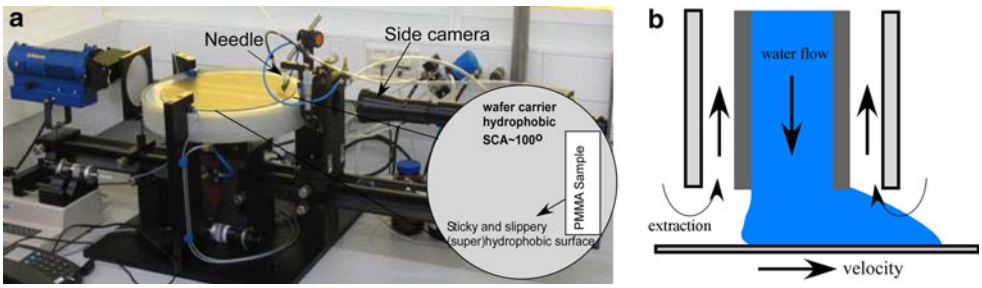

Fig. 2 **a** Turn table setup with the wafer carrier, needle, and side camera, and the illustration showing the wafer carrier with the insert for PMMA sample. **b** schematic of the needle

(Fig. 2a). The ASML system is specifically built to mimic the immersion system used in lithographic scanning tools (Riepen et al. 2008).

The turn table setup is equipped with a direct-drive turn table fixed to a rotary motor which can rotate the 300 mm carrier plate at the maximum velocity of 2.5 m/s ($\sim$160 rpm). The turn table is specifically built to mount the 300-mm wafer. The apparatus is equipped with a needle with two concentric cylinders, the inner one providing fluid and the outer one extracting fluid, thus ensuring a continuous refreshment of water drop (see Fig. 2b). Both supply and extraction are tunable and two flow-controllers allow a real-time monitoring during the experiment. The flow and extraction used for this experiment are 11 and 2200 ml/min, respectively. The liquid remains attached to the needle due to surface tension and the test substrate is rotated by the turn table to impose a relative velocity between the water and the substrate, as illustrated by Fig. 3. The height (h) between the needle and substrate is chosen according to the standards of the immersion system (<500 μm). The meniscus shape of the droplet is captured with a high-speed camera while an imaging tool enables a continuous and simultaneous measurement of both the receding and advancing contact angle as a function of the wafer velocity. The camera image acquisition is triggered by program and a movie file is stored at 10,000 fps during the entire test.

For all the experiments to be described PMMA (poly(methyl)methacrylate) samples were used. Owing to the processing constraints PMMA plates were cut into small samples (7.5 × 2.5 cm^2 size) and mounted on the wafer carrier plate (diameter 300 mm) with the insert (see Fig. 2a). All the experiments were carried out with the needle placed on the PMMA sample and accelerated to specific velocity well within the sample area.

The needle is first placed on the PMMA sample and the flow and extraction valves were opened. The desired acceleration, scan velocity, and distance of travel are programed into the computer-controlled turn table that holds the test substrate. Between each trial, a transverse positioning stage is used to manually locate the needle above a new portion of the sample. The sample is dried using a nitrogen gun to remove any liquid that may have accumulated on the surface. The data acquisition procedure is repeated at increasing scan velocities until steady-state liquid loss is observed, i.e., liquid loss occurring during the constant scan velocity portion of the traverse that is not associated with the acceleration or deceleration portions of the process, as illustrated by Fig. 3. For superhydrophobic samples, high acceleration of up to 80 m/s^2 was used in order to reach the maximum velocity in a short time. Post processing of the images for dynamic contact angles is performed using a LABVIEW program. A separate MATLAB code has been used to verify the velocity of the wafer from the movie file using the motion detection algorithm.

Fabrication of nanotextured hydrophobic and superhydrophobic PMMA surfaces has been described in detail by Tserepi et al. 2005, Vourdas et al. (2007, 2009) and Tsougeni et al. 2009. In brief, optically transparent 2 mm thick PMMA plates were processed in a 13.56 MHz RF plasma etcher with helicon source. The PMMA plates were etched in oxygen plasma to create nanoroughness, followed by fluorocarbon plasma deposition, thus altering the surface chemistry to create a superhydrophobic surface. A thin layer of about 40 nm fluorocarbon was deposited with a deposition time of 45 s (Bayiati et al. 2004).

This study evaluates three different surfaces to compare its dynamic contact line behavior on the turn table system:

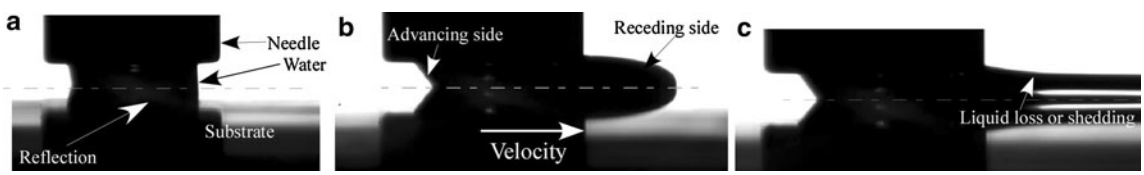

Fig. 3 Water drop with the needle on the top and substrate on the bottom under **a** equilibrium condition, **b** under normal movement with tail formation, and **c** under liquid loss condition

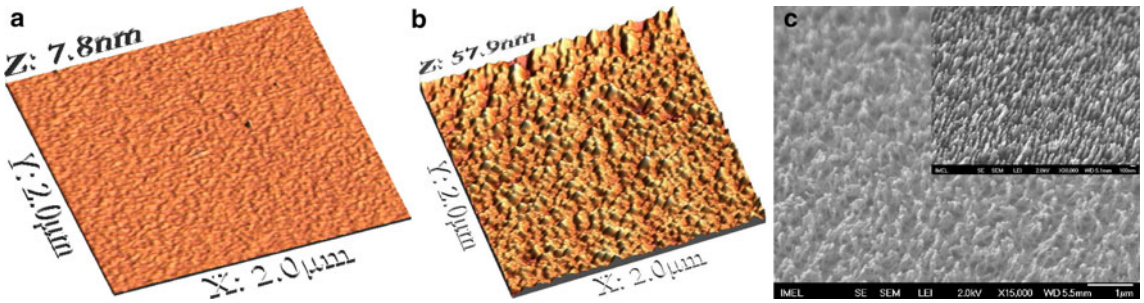

Fig. 4 **a** 3D AFM topology of smooth hydrophobic surface (*Z*-range 7.8 nm, RMS = 0.5 nm). **b** 3D AFM topology of sticky hydrophobic surface (*Z*-range 57.9 nm, RMS ~ 7 nm). **c** SEM micrograph of nanotextured Superhydrophobic PMMA surface (RMS = 70 nm)

(1) Smooth hydrophobic surfaces (see Fig. 4a); (2) sticky (rough) hydrophobic surfaces (see Fig. 4b); and (3) water repellent slippery superhydrophobic surfaces (see Fig. 4c). The smooth hydrophobic surfaces are deposited by just treating a clean PMMA plate in the C_4F_8 plasma. The sticky hydrophobic surfaces are fabricated by etching the PMMA plate for 20 s in oxygen plasma and then depositing a fluorocarbon layer by a C_4F_8 deposition for 45 s. The slippery superhydrophobic surfaces are fabricated by etching the PMMA plate for 2 min and then depositing the fluorocarbon layer. All the samples are optically transparent.

3 Results

Figure 5 shows the drop shape under equilibrium condition when both the flow and extraction are set to the experimental conditions and a refreshing drop is idling on different surfaces. The surface roughness (RMS), static contact angle (SCA), static advancing contact angle (SACA), and static receding contact angle (SRCA) of water drop on various surfaces is shown in Table 1. Figure 5 also shows the dynamic receding contact angle (DRCA) which is the contact angle of the receding meniscus when the drop is continuously refreshed between the needle and substrate. The measured SCA and DRCA values are within the marginal error of ±3. The smooth hydrophobic surface with the SCA of about 110° shows a completely wetting surface beneath the needle. Sticky and slippery surfaces on the other hand show similar DRCA and similar contact line, despite different SCA, SACA, SRCA, and roughness.

Table 1 Surface roughness, static, and receding contact angle (in °) of water on various surfaces

Sample	RMS (nm)	SCA	SACA	SRCA	DRCA
Smooth hydrophobic	0.5	108	110	78 ± 6	83
Sticky hydrophobic	7	145	146	121 ± 4	135
Slippery superhydrophobic	70	152	154	148 ± 5	135

The smooth or nano-textured PMMA sample was placed on the insert in the wafer carrier and the needle was positioned well within the PMMA sample. Figure 6a shows the DRCA-velocity plot for a smooth surface; here the turn table is accelerated to reach the set velocity, while the shape of the drop at the specific velocity is shown in the inset. On the smooth hydrophobic surface, the instability of the receding contact line occurs at the critical velocity ~1 m/s. This is well in agreement with the previous models (*Cox-Voinov*). The receding contact angle starts to decrease from 80° to 40° just before the start of water loss. Figure 6b shows the stable receding contact angle as a function of velocity up to 2.5 m/s on a superhydrophobic surface. To better understand the meniscus behavior as a function of acceleration, a totally different picture is seen on rough hydrophobic and superhydrophobic surfaces as shown in Fig. 7 and 8, respectively, which present the velocity versus time behavior and the drop shapes on such surfaces. On a rough hydrophobic sticky surface, there were no instabilities on the receding contact line even at the system's high velocity 2.5 m/s. Although it is expected to be in the wetting state (Wenzel) still the critical velocity

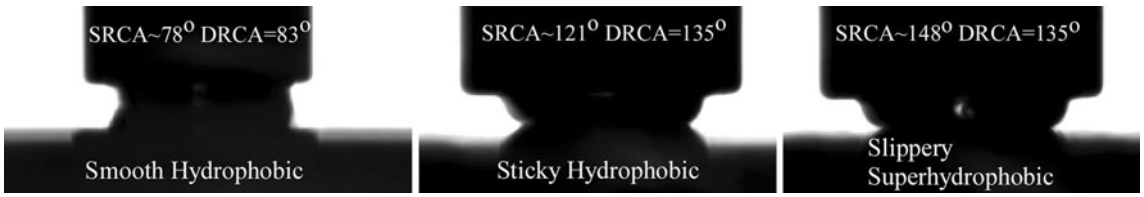

Fig. 5 Drop shape and contact line under equilibrium state with flow/extraction set and the water drop sitting on various surfaces

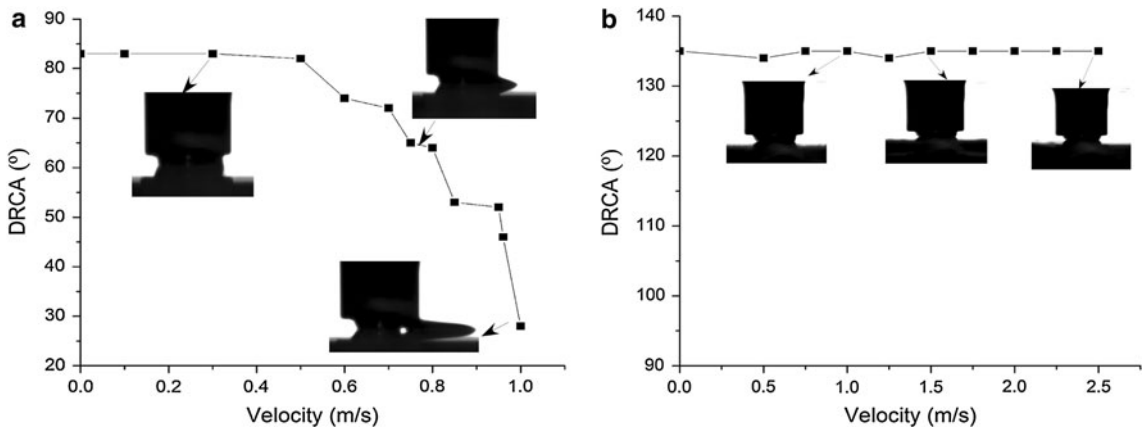

Fig. 6 Dynamic receding contact angle as a function of wafer velocity for **a** smooth hydrophobic surface and **b** superhydrophobic surface

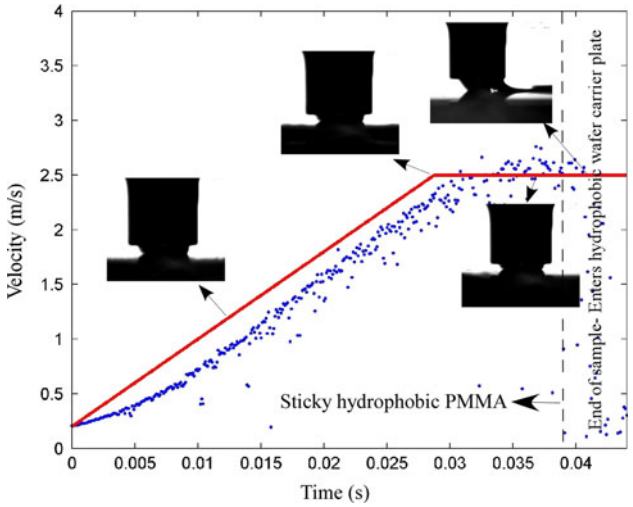

Fig. 7 Velocity versus time plot with the *inset* picture showing the drop shape at different time scale captured from the side camera on the sticky hydrophobic sample

is well above the setups maximum velocity. This is probably because the SRCA is higher compared to a smooth surface (121 versus 78, respectively). In addition, DRCA is higher compared to a smooth surface (135 versus 83, respectively). According to Voinov's equation an increase of the critical velocity by a factor of at least 1.5 is expected $(121/78)^3$ while a factor of at least >4 $(135/83)^3$ is expected based on the DRCA.

Superhydrophobic surface also showed a stable contact line up to 2.5 m/s. A water droplet on the rough hydrophobic and superhydrophobic surface exhibited no difference between an advancing and receding angle (Figs. 7, 8). Since the DRCA were similar between rough hydrophobic and superhydrophobic surfaces the authors saw no differences in their behavior. However, owing to the high value of slip length for superhydrophobic surface, the authors expect to have a higher critical velocity which cannot be reached with the present setup.

Fig. 8 Velocity versus time plot with the *inset* picture showing the drop shape at different time scale captured from the side camera on the slippery superhydrophobic sample

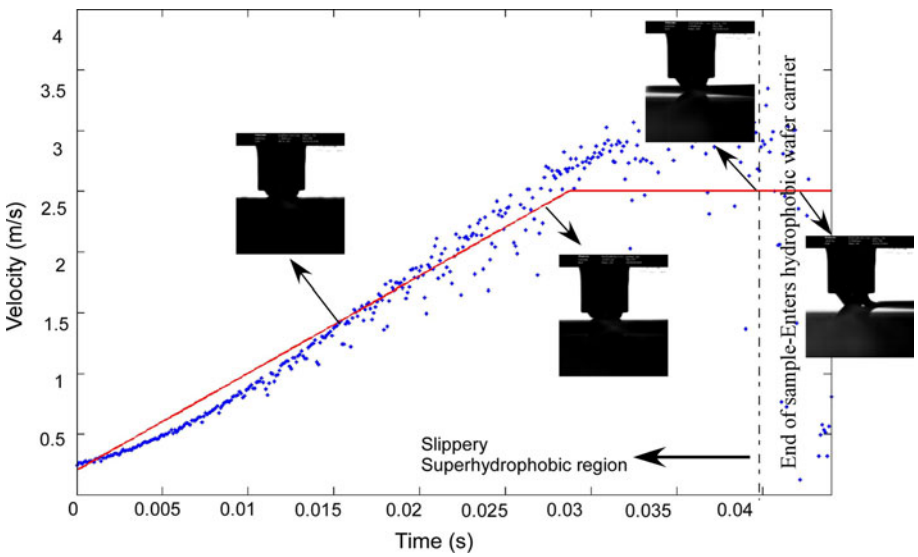

MATLAB code is used to verify the actual velocity of the turntable. The blue dots in the plot indicate the velocity analyzed by image processing with MATLAB. The authors have also observed that instabilities on the receding contact line are unaffected by height between the needle and the sample.

A high rate of acceleration can lead to liquid loss even when the steady state behavior would correspond to a stable receding meniscus. In order to study whether the acceleration has any effect on the liquid loss property, acceleration was increased to see if this has any influence. No acceleration-induced liquid loss was observed on both the sticky and slippery superhydrophobic surface for up to the acceleration of 80 m/s^2. This suggests that acceleration effects may have no significant role for these coatings. Also, since it is suspected that the rough superhydrophobic surface is prone to bubble formation (Checco et al. 2010) the bottom camera directly underneath the needle was focused through the transparent sample on the surface, but no bubble formation was observed.

In conclusion, the data presented show that, for these nanotextured and hydrophobized surfaces, the authors never reach the critical velocity (i.e., no water loss) up to the maximum range of the setup. From Fig. 1, comparing the experimental critical velocity ($V_{cr} = 1$ m/s) for smooth hydrophobic surface (SRCA = 80°, assumed slip length = 10 nm) to the theoretical value, it was found that the theoretical prediction ($V_{cr} \sim 2$ m/s) is two times the experimental value. Provided this factor of 2 (theory/experiment) is also valid for rough surfaces, the critical velocity for the sticky hydrophobic surface (SRCA $\sim$ 121°, assumed slip length $\sim$ 100 nm) is expected to be in the range of 4.5 m/s, which is far larger than the experimental capability. However, work is in progress to produce even less textured surfaces (less receding angle) for which the critical velocity is probably below the maximum velocity allowed by the setup. In addition, the authors are conducting flow measurements in nanotextured microchannels in order to have a better estimate of the slip length and thus more direct comparisons to the theoretical value (see Fig. 1). As far as answering the question why a sticky surface does not show any water loss, the authors can think as follows: The authors hypothesize that the force of extraction overcomes the sticky surface from pinning the water drop (see Fig. 9), and this causes an over performance of the sticky hydrophobic surface. Currently, the authors are forcibly decreasing the air extraction rate to see if water loss will occur.

4 Conclusion

The authors have studied the water contact line behavior on nanotextured hydrophobic and superhydrophobic surfaces, and have shown a dramatic increase in critical velocity over such surfaces. The sticky and slippery superhydrophobic surfaces can be potential candidates that can serve to approximately guide the development of fluid control for immersion systems while maximizing throughput. From these experiments, the authors have shown that sticky and slippery superhydrophobic surfaces show no water loss up to 2.5 m/s. It is also significant to notice that even a small roughness (RMS $\sim$ 7 nm) greatly improves the maximum stable scanning velocity compared to a smooth hydrophobic film, providing a new method to increase and control critical velocity. The authors believe that the increase of contact angle and slip length are the main reasons for such enhanced performance of rough hydrophobic surfaces.

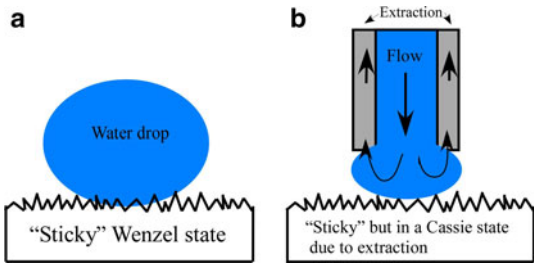

Fig. 9 A hypothesis: water drop on **a** a sticky rough hydrophobic sample in "Wenzel state" under static condition with no extraction and **b** under dynamic substrate with extraction, when the sticky surface looks like a slippery surface (Cassie state)

Acknowledgments Financial support by the FP7 Marie Curie Initial Training Network "Surface Physics for Advanced Manufacturing" project ITN 215723 is kindly acknowledged. Author A.K. Gnanappa would like to thank Koen Winkels (University of Twente) for the help with MATLAB code. The authors also wish to thank Nasos Botsialas (NCSR Demokritos, Athens) for providing micro-drilling of PMMA samples.

References

Bayiati P, Tserepi A, Gogolides E, Misiakos KJ (2004) Selective plasma-induced deposition of fluorocarbon films on metal surfaces for actuation in microfluidics. J Vac Sci Technol A 11:1546–1551

Brandl S, Watso R, Holmes S, Wei Y, Petrillo K, Cummings K, Goodwin F (2006) Investigation of immersion related defects using pre- and post-wet experiments. Proc SPIE 6154:302–310

Burnett H, Shedd T, Nellis G, El-Morsi M, Engelstad R, Garoff S, Varanasi K (2005a) Control of the receding meniscus in Immersion Lithography. J Vac Sci Technol B 23:2611–2616

Burnett H, Shedd T, Nellis G, Van Peski CJ (2005b) Static and dynamic contact angles of water on photoresist. J Vac Sci Technol B 23:2721–2727

Burnett HB, Wei AC, Morsi MS, Shedd TA, Nellis GFJ, Van Peski C, Grenville A (2006) Modeling and experimental investigation of bubble entrapment for flow over topography during immersion lithography. J Microlith Microfab Microsyst 5(1):013008-1–013008-8

Checco A, Hofmann T, DiMasi E, Black T, Ocko BM (2010) Morphology of air nanobubbles trapped at hydrophobic nanopatterned surfaces. Nano Lett 10(4):1354–1358

Choi CH, Kim CJ (2006) Large slip of aqueous liquid flow over a nanoengineered superhydrophobic surface. Phys Rev Lett 96:066001-1–066001-4

Cox RG (1986) The dynamics of the spreading of liquids on a solid surface. Part 1. Viscous flow. J Fluid Mech 168:169–194

Eggers J (2004) Toward a description of contact line motion at higher capillary numbers. Phys Fluids 16:3491–3494

Gogte S, Vorobieff P, Truesdell R, Mammoli A, van Swol F, Shah P, Brinker C (2005) Effective slip on textured superhydrophobic surfaces. J Phys Fluids 17:51701-1–51701-4

Joseph P, Cottin-Bizonne C, Benoit JM, Ybert C, Journet C, Tabeling P, Bocquet L (2006) Slippage of water past superhydrophobic carbon nanotube forests in microchannels. Phys Rev Lett 97:156104-1–156104-4

Mulkens J, Streefkerk B, Jasper H, de Klerk J, de Jong F, Levasier L, Leenders M (2007) Defects, overlay, and focus performance improvements with five generations of immersion exposure systems. Opt Microlithogr XX Proc SPIE 6520:652005-1–652005-11

Niwa T, Enomoto M, Shimura S, Kyoda H, Kawasaki T, Kitano J (2005) Optimization of equipment for 193-nm immersion processing. Adv Resist Technol Process XXII Proc SPIE 5753: 799–806

Petrov PG, Petrov JG (1992) A combined molecular-hydrodynamic approach to wetting kinetics. Langmuir 8:1762–1767

Petrov JG, Sedev RV, Petrov PG (1992) Effect of geometry on steady wetting kinetics and critical velocity of film entrainment. Adv Colloid Interface Sci 38:229–269

Podgorski T, Flesselles JM, Limat L (2001) Corners, cusps, and pearls in running drops. Phys Rev Lett 87:036102-1–036102-4

Riepen M, Evangelista F, Donders S (2008) Contact line dynamics in immersion lithography-dynamic contact angle analysis. In: Proceedings of the 1st European Conference on Microfluidics—Microfluidics 2008, Bologna, December 10–12

Sanders DP (2010) Advances in patterning materials for 193nm immersion lithography. Chem Rev 110(1):321–360

Schuetter SD, Shedd TA, Nellis GFJ (2007) Prediction of the velocity at which separates from a moving contact line. J Micro/Nanolithogr MEMS MOEMS 6(2):023003-1–023003-8

Shedd TA, Schuetter SD, Nellis GF (2006) Experimental characterization of the receding meniscus under conditions associated with immersion lithography. Opt Microlithogr XIX Proc SPIE 6154:61540R-1–61540R-11

Snoeijer JH, Delon G, Fermigier M, Andreotti B (2006) Avoided critical behavior in dynamically forced wetting. Phys Rev Lett 96:174504-1–174504-4

Tserepi A, Gogolides E, Misiakos K, Vlachopoulou ME, Vourdas N (2005/2006) Greek Patent application number 20050100473, PCT application number GR2006/000011

Tsougeni K, Vourdas N, Tserepi A, Gogolides E, Cardinaud C (2009) Mechanism of oxygen plasma nanotexturing of organic polymer surfaces: from stable super hydrophilic to super hydrophobic surfaces. Langmuir 25(19):11748–11759

Voinov OV (1976) Hydrodynamics of wetting. Fluid Dyn 11:714–721

Vourdas N, Tserepi A, Gogolides E (2007) Nanotextured superhydrophobic transparent poly(methyl methacrylate) surfaces using high-density plasma processing. Nanotechnology 18: 125304-1–125304-7

Vourdas N, Vlachopoulou ME, Tserepi A, Gogolides E (2009) Micro and nano structuring and texturing of polymers using plasma processes: potential manufacturing applications. Int J Nanotechnol 6:152–163